HTLV-III_B–producing H9 cells had exerted a substantial cytopathic effect on the YTA1 population by day 6 in culture, and by day 10 the YTA1 population was almost completely killed. The addition of suramin at concentrations of 50 μg/ml or greater enabled the YTA1 target population to survive and grow in the presence of HTLV-III_B. (At concentrations of 100 μg/ml or higher, the drug clearly blocked the cytopathic effect of the virus but did exert an inhibitory effect on the normal target T-cell growth.) Thus, suramin can block the replication of HTLV-III_B in permissive H9 cells and can also inhibit the cytopathic effect of HTLV-III_B on an $OKT4^+$ T-cell clone.

Most of what is known about the clinical pharmacology of suramin derives from its use in the therapy of trypanosomiasis and onchocerciasis. After intravenous injection, the drug combines with serum proteins, and much of it circulates in the blood (*18*). It persists in the bloodstream for very long periods [for example, Hawking (*18*) has suggested that it may be detected up to 6 months], and its excretion in the urine is very slow. The therapeutic regimens in use result in considerable accumulation in the plasma (frequently in excess of 100 μg/ml) (*18, 21*). Indeed, concentrations as high as 340 μg/ml may be reached under some conditions (*18*). These concentrations exceed those found to block the infectivity (Fig. 1) and cytopathic effect (Fig. 2) of HTLV-III in the studies reported here.

The capability of suramin to inhibit the reverse transcriptases of animal retroviruses was reported in 1979 (*15*), and we recently confirmed that this agent can inhibit the reverse transcriptases of diverse retroviruses including that of HTLV-III (*22*). However, the drug is not widely viewed as an agent with antiviral therapeutic potential.

We believe the current results provide a rationale for a carefully monitored experimental trial of suramin in patients with AIDS to determine whether the drug can inhibit HTLV-III replication in vivo, and if so, whether clinical improvement takes place. However, we wish to stress several points. First, suramin has a number of recognized toxicities in human beings (*18, 21*). Renal damage is the most common toxicity, but the drug may be associated with other acute life-threatening reactions, including shock and coma. Second, it is possible that the administration of suramin to patients with AIDS could lead to side effects not currently known, or to unexpectedly severe forms of the known side effects. Third, it is possible that interfering with HTLV-III infection will not substantially benefit patients with late-stage AIDS, since at that point the damage to the immune system might be irreversible. Therefore, there may be a rationale for using this agent for experimental trials early in the disease. Finally, we believe that the administration of this agent should be undertaken only in a research facility capable of monitoring the patient's clinical, immunologic, and virologic status.

HIROAKI MITSUYA
Clinical Oncology Program, National Cancer Institute, Bethesda, Maryland 20205
MIKULAS POPOVIC
Laboratory of Tumor Cell Biology, National Cancer Institute
ROBERT YARCHOAN
SHUZO MATSUSHITA
Clinical Oncology Program, National Cancer Institute
ROBERT C. GALLO
Laboratory of Tumor Cell Biology, National Cancer Institute
SAMUEL BRODER
Clinical Oncology Program, National Cancer Institute

References and Notes

1. M. S. Gottlieb *et al.*, *Morbid. Mortal. Weekly Rep.* **30**, 250 (1981); A. Friedman-Kien *et al.*, *ibid.*, p. 305.
2. M. S. Gottlieb *et al.*, *N. Engl. J. Med.* **305**, 1425 (1981).
3. H. Masur *et al.*, *ibid.*, p. 1431; F. P. Siegal *et al.*, *ibid.*, p. 1439; CDC Task Force on Kaposi's Sarcoma and Opportunistic Infections, *ibid.*, **306**, 248 (1982).
4. M. Essex *et al.*, *Science* **220**, 859 (1983); E. P. Gelmann *et al.*, *ibid.*, p. 862; R. C. Gallo *et al.*, *ibid.*, p. 865; R. C. Gallo, *Cancer Surveys* **3**, 113 (1984).
5. F. Barré-Sinoussi *et al.*, *Science* **220**, 868 (1983).
6. M. Essex *et al.*, *ibid.* **221**, 1061 (1983); B. L. Evatt *et al.*, *Lancet* **1983-II**, 698 (1983).
7. J. Schüpbach, M. G. Sarngadharan, R. C. Gallo, *Science* **224**, 607 (1984).
8. M. Popovic, M. G. Sarngadharan, E. Read, R. C. Gallo, *ibid.*, p. 497.
9. R. C. Gallo *et al.*, *ibid.*, p. 500; J. Schüpbach, M. Popovic, R. V. Gilden, M. A. Gonda, M. G. Sarngadharan, R. C. Gallo, *ibid.*, p. 503; M. G. Sarngadharan, M. Popovic, L. Bruch, R. C. Gallo, *ibid.*, p. 506.
10. S. Z. Salahuddin and R. C. Gallo, unpublished data.
11. J. Schüpbach, V. S. Kalyanaraman, M. G. Sarngadharan, P. A. Bunn, D. W. Blayney, R. C. Gallo, *Lancet* **1984-I**, 302 (1984).
12. R. C. Ting, S. S. Yang, R. C. Gallo, *Nature (London) New Biol.* **236**, 163 (1972).
13. D. Baltimore, *Nature (London)* **226**, 1209 (1970); H. M. Temin and S. Mizutani, *ibid.*, p. 1211.
14. H. Toh, H. Hayashida, T. Miyata, *ibid.* **305**, 827 (1983); R. Patarca and W. A. Haseltine, *ibid.* **309**, 728 (1984).
15. E. de Clercq, *Cancer Lett.* **8**, 9 (1979).
16. B. J. Poiesz, F. W. Ruscetti, A. F. Gazdar, P. A. Bunn, J. D. Minna, R. C. Gallo, *Proc. Natl. Acad. Sci. U.S.A.* **77**, 7415 (1980); B. J. Poiesz, F. W. Ruscetti, M. S. Reitz, V. S. Kalyanaraman, R. C. Gallo, *Nature (London)* **294**, 268 (1981).
17. M. Yoshida, I. Miyoshi, Y. Hinuma, *Proc. Natl. Acad. Sci. U.S.A.* **79**, 2031 (1982); F. Wong-Staal *et al.*, *Nature (London)* **302**, 626 (1983).
18. F. Hawking, *Trans. R. Soc. Trop. Med. Hyg.* **34**, 37 (1940); *Adv. Pharmacol. Chemother.* **15**, 289 (1978).
19. H. Mitsuya, H.-G. Guo, J. Cossman, M. Megson, M. S. Reitz, Jr., S. Broder, *Science* **225**, 1484 (1984).
20. S. Matsushita, H. Mitsuya, S. Broder, unpublished data.
21. B. O. L. Duke, *Bull. W.H.O.* **39**, 157 (1968); H. Fuglsang and J. Anderson, in "Research and Control of Onchocerciasis in the Western Hemisphere" (Scientific publication of the Pan American Health Organization, 1974), No. 298, pp. 54–56; M. H. Satti and R. Kirk, *Bull. W.H.O.* **16**, 531 (1957).
22. L. Arthur, R. Gilden, S. Broder, P. Fischinger, unpublished data; P. Sarin and R. C. Gallo, unpublished data.
23. We thank J. F. Berzofsky and J. Hoofnagle for helpful discussions.

29 August 1984; accepted 11 September 1984

Optical Measurements of Extracellular Calcium Depletion During a Single Heartbeat

Abstract. *The impermeant dye antipyrylazo III was used to measure depletion of extracellular calcium and net influx of calcium through the sarcolemma during the cardiac action potential. It was found that calcium entry occurs continuously during the action potential and is under direct control of the membrane potential. The inotropic action of epinephrine is accompanied by increased influx of calcium, while strophanthidin enhances the twitch without altering calcium influx during the action potential.*

Calcium for activation of contraction in the frog heart is thought to be transported from the extracellular space across the membrane under direct control of the membrane potential (*1–3*). Although a Ca^{2+} current has been identified that contributes to Ca^{2+} transport, its magnitude and its time and voltage dependence do not correspond fully to those of the tension generated (*4, 5*). It has been suggested, therefore, that activator Ca^{2+} is in part released from intracellular pools (*6*) or that it enters the cell through coupled transport systems (*7–9*). To examine these possibilities we used an impermeant Ca^{2+}-sensitive dye, antipyrylazo III (*10*), to measure depletion of Ca^{2+} from the extracellular space. Depletion of Ca^{2+} is assumed to represent net influx of the ion, since equilibration of the extracellular space with the perfusate is a slow process (time constant, 60 to 90 seconds) (*11, 12*). We found that Ca^{2+} enters the cell continuously during the action potential and does so in sufficient quantity to generate tension. The rapid onset of the depletion signal and its enhancement during the inotropic action of epinephrine suggest that Ca^{2+} influx occurs, in part, through the Ca^{2+} chan-

nel. Potentiation of tension with strophanthidin did not increase the Ca^{2+} depletion signal, as predicted on the basis of Na^+ pump inhibition and Na^+-Ca^{2+} exchange (*9, 13–15*). Our experiments give a direct measure of net influx of Ca^{2+} across the sarcolemma during the action potential and suggest that activator Ca^{2+} enters the cell primarily through a maintained or slowly inactivating Ca^{2+} channel.

Calcium depletion was determined from measurements of transmitted light at three different wavelengths (Fig. 1). The measurements were made in a single sucrose gap chamber in which strips of frog ventricle 0.5 to 0.8 mm in diameter were mounted with one end attached to an isometric force transducer (*1*). Light absorption by the strip and the perfusate was measured by shining a beam through the movable, transparent walls of the perfusion chamber. Gentle compression of the strip between these walls reduced artifacts that might have been caused by the motion of contraction. Contraction artifacts were further reduced by using Ringer solution with a low concentration of Ca^{2+} (0.05 to 0.2 m*M*) and by summing the depletion signal at a given wavelength with signals measured simultaneously at 600 and 788 nm [antipyrylazo III has an isosbestic point at 600 nm and is transparent at 788 nm (*16*)].

Figure 1, A and B, shows changes in absorption occurring during the action potential before and after addition of antipyrylazo III. Without dye (Fig. 1A) the three absorption measurements gave a flat weighted average signal. In muscles perfused with dye-containing solution (Fig. 1B) there was a pronounced Ca^{2+} depletion signal during the action potential. The signal returned to baseline long after repolarization or relaxation of the tension. Although the contraction-induced optical signals at 600 and 788 nm are about 25 percent of the Ca^{2+} signal, the weighing procedure suppressed them—generally by a factor of 10 or more (Fig. 1A), yielding a signal virtually free of contraction artifacts (less than 5 percent).

Figure 1C shows that the weighing procedure produces a similar Ca^{2+} depletion signal even when the uncompensated contraction artifacts are comparable to or larger than the Ca^{2+}-related signal. Such records demonstrate that the weighing procedure can suppress fairly large contraction-induced scattering of light. However, to attain optimal accuracy, we performed experiments only with those preparations in which the uncompensated contraction artifacts were markedly smaller than the Ca^{2+}-related signal.

The wavelength dependence of the Ca^{2+} depletion signal was measured routinely (Fig. 1, D to G) to substantiate that the dye in the extracellular space had an action spectrum similar to that of the dye in a cuvette. Signals at 540, 660, and 718 nm had similar wave forms, but the signal was inverted at 540 nm (below the isosbestic point) and was larger at 660 nm than at 718 nm (Fig. 1, E to G). In Fig. 1D these findings and those from other wavelengths are compared to the Ca^{2+}-related difference spectrum measured with samples of the perfusate in a cuvette. The experimental points are in agreement with the spectrophotometric measurements (continuous curves) when scaled by factors that determine the calibration of the Ca^{2+} depletion signals. As a first step in the calibration procedure we determined the optical path through the extracellular space from the increase in absorption that resulted from admission of the dye-containing perfusate. The Ca^{2+}-induced difference spectra of the perfusate were then normalized to represent a cuvette with the same optical path (0.015 cm). Finally, the changes in absorption measured during the twitch were scaled to give a best fit with the curve (0.6) representing a 400-μM reduction in total Ca^{2+} concentration. For example, the values corresponding to peak depletion were multiplied by 17.8 to match this curve. This indicates a net Ca^{2+} depletion of 400/17.8 μM = 22 μM, or 28 μM considering the nonlinear Ca^{2+} binding of antipyrylazo III.

Spectra similar to those in Fig. 2 were recorded after the twitch tension was markedly suppressed by hypertonic solutions. Tetramethylmurexide and arsenazo I (*17, 18*) produced similar Ca^{2+} depletion signals but were found to be less sensitive than antipyrylazo III. These results suggest that this technique reliably measures the time course and magnitude of Ca^{2+} depletion from the extracellular space.

Onset of the depletion signal occurred in less than 10 msec (compared to 100 msec for the onset of tension) (Fig. 2A).

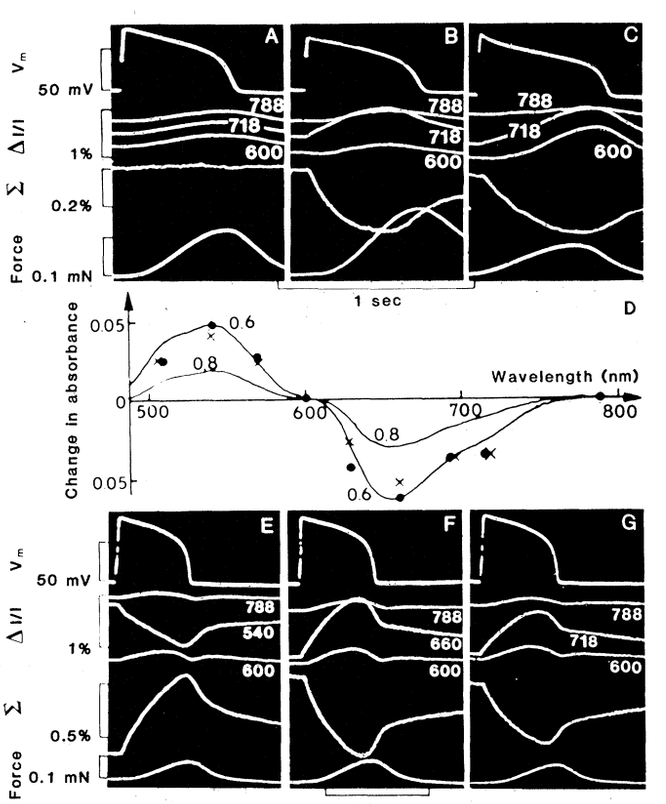

Fig. 1. Sample measurements of extracellular Ca^{2+}. From top to bottom each record shows the action potential (V_m) measured across the sucrose gap, light intensities ($\Delta I/I$) at three wavelengths (in nanometers), a weighted average of these three signals (Σ), and twitch force. (A and B) Measurements in the absence (A) and presence (B) of antipyrylazo III. The concentration of Ca^{2+} in the perfusate was 0.05 m*M* in the preparation represented in (A). This matched the free Ca^{2+} concentration in the preparation represented in (B), in which 3 m*M* antipyrylazo III was added to Ringer solution with a total Ca^{2+} concentration of 1 m*M*. The Ringer solution also contained 116 m*M* NaCl and 3 m*M* KCl and was buffered to *p*H 7.0 to suppress any signals resulting from H^+ fluxes. Magnesium, which would reduce sensitivity, was not present in the perfusate. (C) Similar depletion signal, obtained when uncompensated contraction artifacts were equal to or greater than the Ca^{2+}-related signal. (D to G) Wavelength dependence of the Ca^{2+} signal. The continuous curves in (D) are differential spectra of the perfusate obtained by reducing the total Ca^{2+} concentration from 1 to 0.8 m*M* (0.8) and 1 to 0.6 m*M* (0.6). The symbols correspond to Ca^{2+} depletion signals measured during the twitch at discrete wavelengths in normal Ringer [(●) peak depletion and (x) initial rate of depletion]. Data points were scaled to obtain the best fit with the continuous curve (0.6) representing a 400-μM reduction in Ca^{2+}. Measurements were taken at 540 nm (E), 660 nm (F), and 718 nm (G). Comparison of (B), (C), and (G) shows that, while the contraction artifacts at 600 and 788 nm vary in shape and magnitude from experiment to experiment, the Ca^{2+} depletion signal maintains a characteristic shape.

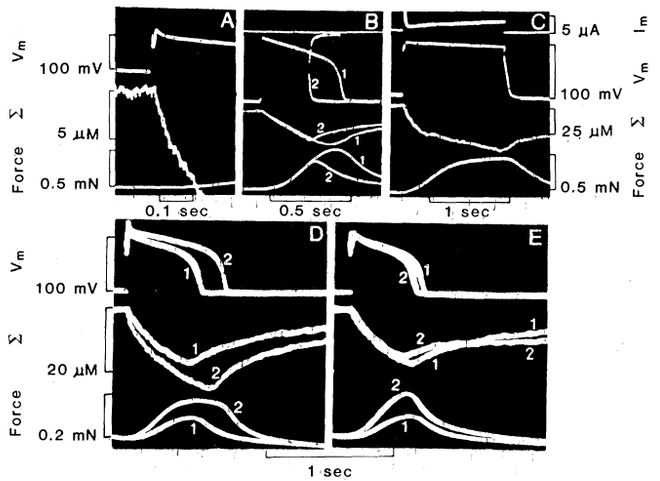

Fig. 2. Effects of membrane potential and drugs on the extracellular Ca^{2+} depletion signal. (A) The rate of Ca^{2+} depletion (Σ) was maximal within 10 msec of depolarization (V_m) and before any force development. In (B) and (C) V_m is the membrane potential measured with a microelectrode and I_m is the membrane current. In (B) the depletion process is promptly terminated when the action potential (trace 1) is stopped by clamping the membrane potential back to the resting potential (trace 2). In (C) the Ca^{2+} depletion signal is maintained for the duration of the depolarization. (D and E) Effect of $10^{-6}M$ epinephrine (D) and $10^{-6}M$ strophanthidin (E) on the depletion signal. Each panel shows action potentials measured across the sucrose gap, the Ca^{2+} depletion signal, and the twitch force recorded in the absence (traces 1) and presence (traces 2) of the drug. Although both drugs potentiated the twitch, only epinephrine enhanced Ca^{2+} influx. The signals were measured at a wavelength of 718 nm.

The rate of depletion was highest at the beginning of the action potential, decreasing slowly during the plateau. The peak depletion value was reached before the onset of repolarization. After termination of repolarization, reaccumulation of Ca^{2+} generally had a small rapid phase, but most of the Ca^{2+} seemed to return to the extracellular space long after relaxation was complete. This suggests that the first step in sequestration of Ca^{2+} is uptake of Ca^{2+} into an intracellular compartment.

Both the depletion signal and developed tension were abbreviated when the action potential was terminated prematurely by a voltage clamp pulse (Fig. 2B). On the other hand, prolonged depolarizations showed that Ca^{2+} did not return to the extracellular space until repolarization had occurred (Fig. 2C). These findings indicate that transsarcolemmal transport of Ca^{2+} and development of tension are under direct control of the membrane potential.

Figure 2, D and E, shows measurements of extracellular Ca^{2+} depletion as the force of contraction was potentiated by epinephrine and strophanthidin. The epinephrine-induced enhancement of contraction and action potential were accompanied by increased Ca^{2+} depletion (Fig. 2D), while potentiation of tension by strophanthidin did not significantly alter the rate of Ca^{2+} depletion (Fig. 2E). These effects were always reversible. In five different ventricular strips epinephrine enhanced the peak Ca^{2+} depletion signal 2.16 ± 0.68 times (mean ± standard deviation) and the twitch tension 1.87 ± 0.63 times, while strophanthidin increased the twitch force 1.94 ± 0.50 times but did not affect the rate of Ca^{2+} depletion. These findings indicate that, while the inotropic effect of epinephrine is mediated by enhanced transsarcolemmal influx of Ca^{2+}, the potentiation of tension by strophanthidin is not. These results do not, however, rule out an altered Ca^{2+} balance between the sarcoplasm and internal Ca^{2+} pools or slow elevations in baseline intracellular Ca^{2+} activity (*19*) induced by the drug.

Our results show that Ca^{2+} indicator dyes, when used as extracellular probes, can rapidly and accurately monitor the time course and magnitude of Ca^{2+} influx after stepped changes in the membrane potential. The rapid response of the dye to changes in Ca^{2+} provides a major advantage over the slower electrode technique (*20, 21*). Simultaneous measurements of absorption at three wavelengths appear to eliminate problems arising from motion-induced light scattering and make it possible to monitor the time course of the Ca^{2+} depletion signal not only after prolonged activity (*22*) but also during contraction. Unlike the electrode method the optical technique measures an average value of Ca^{2+} depletion throughout the different parts of the extracellular space. Thus it seems likely that the depletion occurs first in the subendothelial fraction and only later (and to a lesser extent) in the space between the trabeculae (*23, 24*). It may be that part of the Ca^{2+} signal is related to movement of Ca^{2+} between the various components of the extracellular space and to inhomogeneous distribution of dye. It should be noted, however, that Ca^{2+} depletion occurred very soon after the onset of depolarization (Fig. 2A). Furthermore, the rate of depletion remained fairly constant during the hours of experimentation. These findings suggest that the dye must readily penetrate to the portion of the extracellular space that is adjacent to the myocardial cell membrane.

It should also be noted that the concentration of the dye was such that local changes in total Ca^{2+} concentration could be large without exceeding the linear range of the dye-Ca^{2+} interaction. The change in absorption produced by reducing total Ca^{2+} concentration by 400 μM was only slightly more than twice that resulting from a 200-μM reduction (Fig. 2D). This implies that the optical technique would not distinguish between a large but localized depletion and uniform removal of the same amount of Ca^{2+} from the entire extracellular space. We believe, therefore, that this technique measures the total amount of Ca^{2+} in the extracellular space. The final level of extracellular Ca^{2+} depletion ranged from 15 to 50 μM per beat. With an extracellular space of 25 percent this corresponds to an increase in cellular Ca^{2+} of 5 to 17 μM. This value is markedly larger than most estimates of Ca^{2+} influx based on ^{45}Ca fluxes or voltage clamp currents (*13*), and it appears sufficient (*25*) to account for the relatively modest contraction measured in our Ca^{2+}-poor (0.05 to 0.2 mM) solutions.

Maximum rate of depletion of extracellular Ca^{2+} occurs shortly after depolarization (Fig. 2A) and is enhanced by epinephrine (Fig. 2D). This suggests that part of the depletion is attributable to entry of Ca^{2+} through the slow inward channel (*26, 27*). There is, however, a discrepancy between the published time course of the slow inward current (*28, 29*) and our finding that Ca^{2+} depletion continues throughout depolarization. This suggests that inactivation of the channel is much slower (*30, 31*) or that Ca^{2+} influx occurs by means of a slower countertransport mechanism. That strophanthidin did not increase Ca^{2+} influx as it potentiated the force of contraction puts some limitations on the contribution of a Na^+-Ca^{2+} countertransporter to the influx of Ca^{2+} during a normal twitch (*9, 14*). However, if potentiation of tension by strophanthidin occurs secondary to a slow increase in baseline intracellular Ca^{2+}, this technique would not detect it.

We believe that this technique provides not only an accurate and rapid method for monitoring the time course and magnitude of Ca^{2+} influx during a

single action potential, but also makes it possible to separate and measure the contributions of various Ca^{2+} transport systems to generation of muscle tension.

L. CLEEMANN
G. PIZARRO, M. MORAD
Department of Physiology, University of Pennsylvania, Philadelphia 19104, and Mount Desert Island Biological Laboratory, Salsbury Cove, Maine

References and Notes

1. M. Morad and R. K. Orkand, *J. Physiol. (London)* **219**, 167 (1971).
2. A. Fabiato and F. Fabiato, *Ann. N.Y. Acad. Sci.* **307**, 491 (1978).
3. M. Morad, Y. E. Goldman, D. R. Trentham, *Nature (London)* **304**, 635 (1983).
4. T. Klitzner and M. Morad, *Pfluegers Arch.* **398**, 274 (1983).
5. G. Vassort and O. Rougier, *ibid.* **331**, 191 (1972).
6. R. Niedergerke and S. Page, *Proc. R. Soc. London* **213**, 303 (1981).
7. G. A. Langer, *Annu. Rev. Physiol.* **35**, 55 (1973).
8. M. Horackova and G. Vassort, *J. Gen. Physiol.* **73**, 403 (1979).
9. L. J. Mullins, *Ion Transport in Heart* (Raven, New York, 1981).
10. A. Scarpa, F. J. Brinley, Jr., G. Dubyak, *Biochemistry* **17**, 1378 (1978).
11. R. P. Kline and M. Morad, *Biophys. J.* **16**, 367 (1976).
12. M. Morad, S. Reeck, M. Rao, *Science* **211**, 485 (1981).
13. R. A. Chapman, *Prog. Biophys. Mol. Biol.* **35**, 1 (1979).
14. G. A. Langer, *J. Mol. Cell. Cardiol.* **15**, 647 (1983).
15. S. S. Sheu and H. A. Fozzard, *J. Gen. Physiol.* **80**, 325 (1982).
16. In Fig. 1, A to C and G, the weighted average is $\Sigma = 0.20\ (\Delta I_{600}/I_{600}) - (\Delta I_{718}/I_{718}) + 0.85\ (\Delta I_{788}/I_{788})$, where $\Delta I/I$ is the relative change in light intensity and subscripts are wavelengths in nanometers. The weight chosen for the Ca^{2+} signal (in this case, 718 nm) is −1. The two other weights are calculated by making the simplifying assumption that the contraction artifact of the perfusate or the tissue at any wavelength is proportional to their respective absorptions. Thus, at 600 nm the weight is 1/5 = 0.2 since the dye absorption is five times larger than at 718 nm. At 788 nm the dye is transparent and a weight of 0.85 is calculated to compensate for tissue motion at the two other wavelengths (tissue absorption is roughly proportional to the inverse square of the wavelengths). Different weights were used when the wavelengths or the composition of the perfusate were altered.
17. J. R. Blinks, W. G. Wier, P. Hess, F. G. Prendergast, *Prog. Biophys. Mol. Biol.* **40**, 1 (1982).
18. S. M. Baylor, in *Handbook of Physiology* (Williams & Wilkins, Baltimore, 1983), sect. 10, pp. 355–379.
19. C. O. Lee, D. Y. Uhm, K. Dresdner, *Science* **209**, 699 (1980).
20. K. Dresdner, R. P. Kline, J. Kupersmith, *Biophys. J.* **37**, 239a (1982).
21. D. M. Bers, *Am. J. Physiol.* **244**, H462 (1983).
22. D. W. Hilgemann, M. J. Delay, G. A. Langer, *Circ. Res.* **53**, 779 (1983).
23. S. G. Page and R. Niedergerke, *J. Cell. Sci.* **2**, 179 (1972).
24. L. Cleemann and M. Morad, *J. Physiol. (London)* **286**, 83 (1979).
25. R. J. Solaro, R. M. Wise, J. S. Shiner, F. N. Briggs, *Circ. Res.* **34**, 525 (1974).
26. G. W. Beeler, Jr., and H. Reuter, *J. Physiol. (London)* **207**, 211 (1970).
27. O. Rougier *et al.*, *Pfluegers Arch.* **308**, 91 (1969).
28. E. Coraboeuf, in *The Slow Inward Current in Cardiac Arrythmias*, D. P. Zipes, J. C. Bailey, V. Elharran, Eds. (Nijhoff, The Hague, 1980).
29. K. S. Lee and R. W. Tsien, *Nature (London)* **297**, 498 (1982).
30. R. S. Kass and T. Sheuer, *J. Mol. Cell. Cardiol.* **14**, 615 (1982).
31. M. Morad and L. Tung, *Am. J. Cardiol.* **49**, 584 (1982).
32. Supported by the W. W. Smith Foundation and NIH grant HL16152. We thank S. Baylor, G. Dubyak, and T. Scarpa for many helpful suggestions.

22 May 1984; accepted 25 July 1984

Expression of the 3′ Terminal Region of Human T-Cell Leukemia Viruses

Abstract. *Human T-cell leukemia viruses (HTLV) are closely associated with some human T-cell leukemias and lymphomas. A unique 3′ region of the HTLV genome is believed to be involved in HTLV-induced cellular transformation, although the function of this region has yet to be determined. A subgenomic messenger RNA transcribed from this region of HTLV has now been characterized. These results provide direct evidence for the expression of a novel gene in HTLV.*

The human T-cell leukemia viruses (HTLV) types I and II are lymphotropic retroviruses that have been isolated from patients with specific T-cell malignancies (*1–4*). Infection of normal leukocytes by HTLV-I or HTLV-II in vitro results in the transformation of mature T cells, as shown by their continued proliferation (*5–8*). The mechanism of HTLV-induced leukemogenesis remains obscure. No known viral oncogene has been identified in HTLV. However, analyses of HTLV-I and HTLV-II nucleic acid sequences have identified a region, termed X, whose function is, as yet, unknown (*9–11*). The X region is bounded by *env* and the 3′ terminal repeat (LTR), is approximately 1.6 kilobase pairs long, and contains several open reading frames. The conservation of the X sequence in both HTLV-I and HTLV-II suggests that it encodes a protein that may play a critical role in HTLV replication or HTLV-induced cellular transformation, or both.

The HTLV-II–infected Mo-T cell line was established by primary culture of splenic tissue from a patient with a T-cell variant hairy cell leukemia (*12, 13*). Mo-T cell RNA was assayed for the presence of X-specific sequences by the hybridization–S_1 nuclease technique. Nucleic acid sequence analyses of the HTLV X region revealed three open reading frames in HTLV-II (X-a to X-c) and four open reading frames in HTLV-I (X-I to X-IV) (*9–11*). Three of the open reading frames in HTLV-I are homologous with those in HTLV-II, namely, X-II with X-a, X-III with X-b, and X-IV with X-c. Comparison of nucleic acid sequences in the X region of HTLV-I and HTLV-II reveals only 33 percent homology in the first third of the sequences and an abrupt shift to 75 percent homology in the 3′ two-thirds, where the homologous open reading frames are located (*10, 11*). The Hha I–Cla I probe prepared from cloned HTLV-II DNA (see Fig. 1B) is a 431-base-pair fragment that spans the junc-

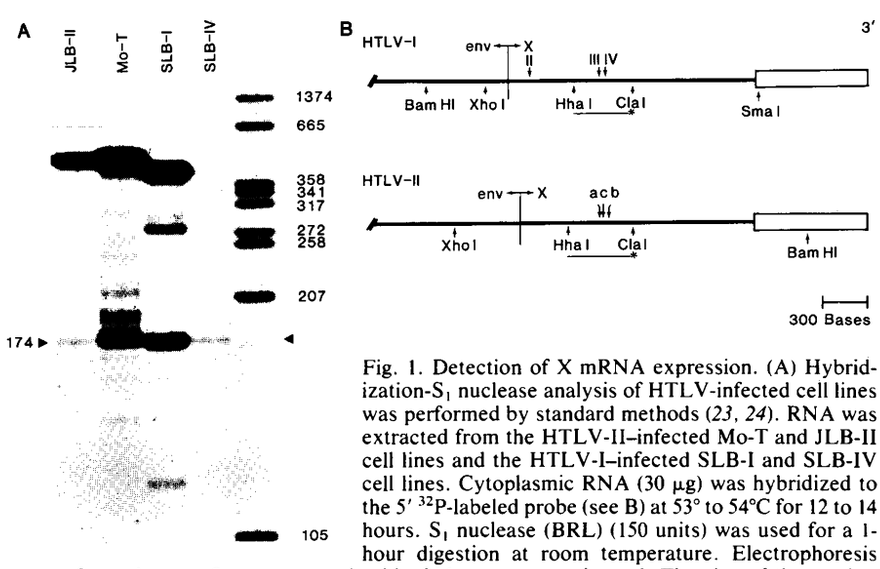

Fig. 1. Detection of X mRNA expression. (A) Hybridization-S_1 nuclease analysis of HTLV-infected cell lines was performed by standard methods (*23, 24*). RNA was extracted from the HTLV-II–infected Mo-T and JLB-II cell lines and the HTLV-I–infected SLB-I and SLB-IV cell lines. Cytoplasmic RNA (30 μg) was hybridized to the 5′ ^{32}P-labeled probe (see B) at 53° to 54°C for 12 to 14 hours. S_1 nuclease (BRL) (150 units) was used for a 1-hour digestion at room temperature. Electrophoresis was performed on an 8 percent acrylamide–8*M* urea sequencing gel. The size of the marker DNA fragments is shown in nucleotides. The 174-base fragment is indicated by the arrow. Control S_1 nuclease studies with RNA from uninfected cells and either HTLV probe reveal no protected DNA fragment (data not shown). (B) Partial restriction enzyme map of the pHT-1 HTLV-I and pH-6 HTLV-II DNA clones. The 3′ long terminal repeat is shown by an open box. The division between X and *env* sequences is indicated. The 5′ ends of the open reading frames are shown for HTLV-I X-II, X-III, and X-IV and for HTLV-II X-a, X-b, and X-c. The Hha I–Cla I hybridization probe utilized for S_1 nuclease analysis is shown as a thin line below the map with an asterisk denoting the site of 5′ ^{32}P-labeling. The sizes of the HTLV-I pHT-1 and HTLV-II pH-6 probes are 396 and 431 nucleotides, respectively.